Kinetics of optically excited charge carriers at the GaN surface

A. Winnerl, R. N. Pereira, and M. Stutzmann

Walter Schottky Institut and Physik Department, Technische Universität München, Am Coulombwall 4, 85748 Garching, Germany

(Received 19 September 2014; revised manuscript received 22 December 2014; published 26 February 2015)

In this work, we combine conductance and contact potential difference measurements in a consistent and systematic way, in steady-state and transient modes, both in the dark and under illumination. With this we obtain valuable information about the kinetics of charges at and close to the surface of GaN. We compare the processes involved in the accumulation and the decay of charge carriers generated via excitation with above and below band-gap light with varying light intensity. In particular, we probed the role played by localized defect states in the kinetics of photogenerated charges. These states are responsible for the trapping of photogenerated electrons in the space-charge region close to the surface, which explains the slow response of the photocurrent to illumination. These states are also involved in the transfer of electrons back to the surface after illumination, which results in the slow recovery of the photocurrent and the contact potential difference in the dark.

DOI: 10.1103/PhysRevB.91.075316 PACS number(s): 81.05.Ea, 73.61.Ey, 78.66.Fd, 73.25.+i

I. INTRODUCTION

The III-nitride materials system consists of the III-V compound semiconductors aluminum nitride (AlN), gallium nitride (GaN), and indium nitride (InN) and their ternary or quaternary compounds. This material system is widely used in light-emitting diodes [1], high-power and high-temperature electronic devices [2], and short-wavelength photodetectors [3]. More recently, III-nitrides have been attracting interest in the fields of photoelectrochemistry and photocatalysis [4–7]. The flexibility in alloying and doping of the III-nitride materials is expected to provide an unprecedented control over the electronic properties of the surface. For example, the effective surface work function may be tuned in the range from 0 to 6 eV, spanning almost all relevant redox levels in photoelectrochemistry [8].

The transport and recombination of photogenerated charge carriers is important for many current applications of GaN, but are particularly important in the case of photocatalysis, since this is a surface-related phenomenon. The absorption of light in a semiconductor creates free electrons and holes in the bulk and close to the surface. Electrons (holes) reaching the surface can promote reduction (oxidation) reactions. The efficiency of the photocatalytic activity depends on the efficiency of separation of photogenerated electrons and holes and on the migration of the required charges to the surface. The trapping or recombination of these charges within the bulk or at unwanted defects will reduce the photocatalytic activity.

A large number of studies can be found in the literature dedicated to the investigation of surface-related effects on GaN using various techniques such as photoluminescence [9–11], photoconductivity [12–17], and contact potential difference measurements [18–22]. In the dark, *n*-type GaN grown on *c*-plane sapphire shows an upward band bending of approximately 1 eV due to trapping of electrons at surface states [23–26], which results in the formation of a positive space-charge region (SCR) close to the GaN surface. The origin of the electron acceptor surface states is still not well understood. As in other semiconductors, these states may be related to intrinsic defects such as dangling bonds, impurities, surface reconstruction, or random stress [27–30]. They may also originate from extrinsic sources such as atoms or molecules adsorbed on the surface or defects in a surface oxide layer. For GaN it is known that oxygen is chemisorbed at the surface [23] and that a thin oxide layer is formed [31,32]. Under illumination with ultraviolet (UV) light, the band bending can be reduced by 0.3–1.1 eV, corresponding to the so-called surface photovoltage (SPV) [11,32–34]. The SPV has been measured in many studies which have used various techniques, such as x-ray photoelectron spectroscopy (XPS) [33,35], Kelvin probe force microscopy (KPFM) [22,34], and the macroscopic Kelvin probe technique [11,18–21,32,36]. In these studies, it has been discussed that photogenerated electrons and holes are separated by the built-in electric field caused by the surface band bending. It is considered that the separated holes drift to the surface, resulting in a reduction of the surface charge density and of the surface band bending, whereas the corresponding electrons drift through conduction band (CB) states to the bulk. Another common feature of previous studies of SPV is that they explain the observed slow recovery of the surface band bending after switching off the illumination by considering that the surface charge density is restored to its dark value by thermionic transfer of CB electrons to the surface states over the energy barrier defined by the surface band bending. This process has also been used to explain why the photocurrent in GaN persists for a very long time after the illumination has been turned off [12,13,36], a phenomenon known as persistent photoconductivity (PPC) [14–17]. The origin of the PPC is still under discussion and different models have been considered to explain its origin, such as trapping at defects with bistable character [14,17], AX or DX centers [37–39], random potential fluctuations due to nonstoichiometry [40], defects at heterointerfaces [15], and unintentional incorporation of a cubic crystal phase in hexagonal GaN [41]. A possible correlation between the PPC and the yellow luminescence (YL), commonly observed in GaN, has also been suggested in some reports and seen as an indication that bistable defects are the origin of both PPC and YL [9,10,17]. However, other reports do not see a correlation between these two phenomena [15,40,42].

In spite of the numerous investigations, there is still not a consensual understanding of the physical processes involving charges photogenerated close to the GaN surface that could,

for example, explain coherently both the SPV and PPC phenomena. In this work, we combine conductance (PC) and contact potential difference (CPD) measurements in a consistent and systematic way to identify the main processes involved in the kinetics of charges photogenerated at and close to the GaN surface. For instance, by comparing PC and CPD data recorded in steady-state and transient modes, both in the dark and under illumination, we unveil the central role played by localized defect states in the trapping and transport of charges photogenerated close to the GaN surface. From both qualitative and quantitative analyses of our data, we conclude that charge hopping via localized states, rather than thermionic emission, is the dominant process involved in the back transfer of CB electrons to surface states when photoexcitation is ceased. This process governs both the PPC and the slow decay of SPV commonly observed in GaN.

II. EXPERIMENTAL DETAILS

Metal-organic chemical vapor deposition (MOCVD) grown (0001) GaN layers on sapphire with a thickness of 3.5 μm, unintentionally n-type doped, were purchased from Lumilog. These GaN layers exhibit a carrier concentration of 1.4×10^{17} cm^{-3} and an electron mobility of 170 cm^2/Vs measured by Hall effect in the van der Pauw geometry. Ohmic top contacts (Ti/Al/Ti/Au, 20/80/10/90 nm) were deposited by electron beam evaporation and annealed in nitrogen for 5 min at 1023 K. The annealing was carried out to ensure stable contacts. From Hall measurements performed before and after annealing of the contacts we observed that the carrier concentration and charge mobility were not affected by the annealing within the experimental error of the measurements. Conductance and contact potential difference measurements in steady-state and transient modes, both in the dark and under illumination, were performed on these samples. All measurements were performed in air and at room temperature. For the illumination, UV light-emitting diode arrays with two different wavelengths (270 and 342 nm) were used. The CPD was measured by the Kelvin probe technique [43] using a commercial Kelvin Probe S system and a Kelvin Control 07 (Besocke Delta Phi). The metal reference electrode was a piezoelectrically driven gold grid with a diameter of 3 mm and a work function of 4.9 eV. The conductance measurements were performed with a homemade system consisting of measurement probes (Cascade Mictrotech) and a dual channel sourcemeter (Keithley 2612B) for measuring the current through the sample and driving the light-emitting diodes. The time resolution of the CPD and the PC measurements is limited by the time interval of reading out the signals with sufficient signal-to-noise ratio and is approximately 0.15 s in both cases. CPD measurements on a microscopic scale were performed with a commercial MultiMode 8 AFM System (Bruker) in the Peak Force KPFM mode.

III. RESULTS AND DISCUSSION

CPD is the difference between the work functions of a metal reference electrode ($e\Phi_M$) and a semiconductor surface ($e\Phi_{SC}$):

$$eU_{CDP} = e(\Phi_M - \Phi_{SC}).$$

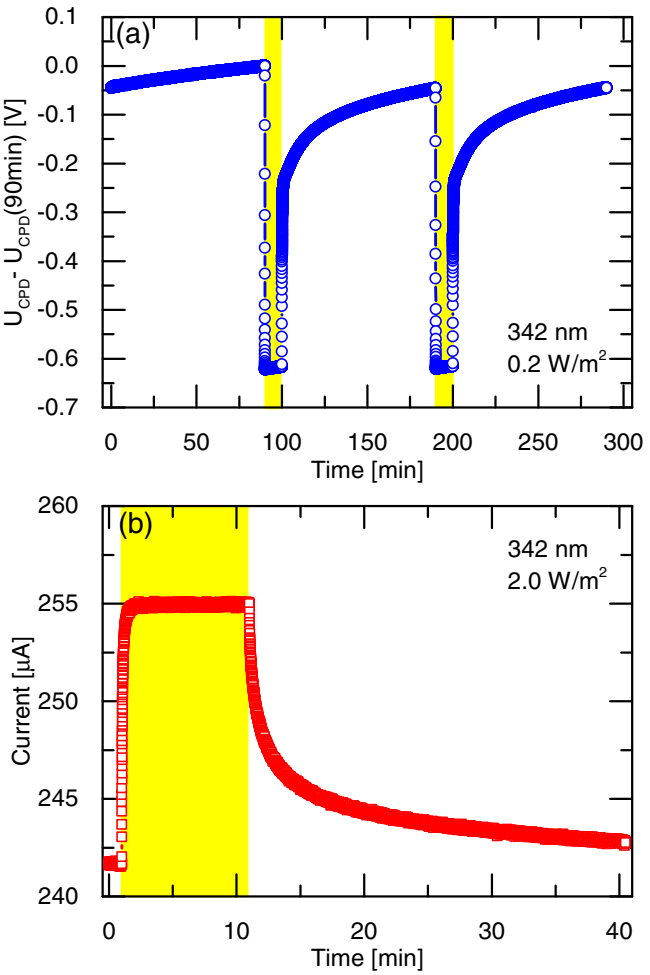

FIG. 1. (Color online) (a) CPD and (b) current recorded as a function of time. The illumination time intervals are highlighted in yellow.

In a typical CPD measurement, the CPD signal $U_{CDP}(t)$ is measured as a function of time t. Under illumination, electron-hole pairs are generated, resulting in a charge redistribution within the sample, which leads to changes of charge density in the SCR and at the surface. The corresponding photoinduced change in the CPD signal, the difference of the CPD signal in the dark U_{CPD}^{dark} and under illumination U_{CPD}^{illum}, is the surface photovoltage (SPV). Thus, the SPV corresponds to the change in the surface band bending and enables the direct measurement of charge exchange between the SCR and the surface.

In this work, a typical CPD measurement consists of two illumination cycles as can be seen in Fig. 1(a). First, the measurement is carried out in the dark, until the CPD signal is constant. Then, the sample is illuminated until the CPD signal saturates. For all light intensities, 10 min of illumination were long enough for the CPD signal to saturate under illumination. For the applied light intensities, the decay of the CPD signal in the dark after illumination was measured for 90 min. This provided enough data for a meaningful fit of the decay of the CPD signal in the dark.

The decay of the CPD signal in the dark after illumination could be well described by a sum of two stretched exponential

functions

$$U_{\mathrm{CDP}}(t) = A_1 e^{-\left(\frac{t}{B_1}\right)^{C_1}} + A_2 e^{-\left(\frac{t}{B_2}\right)^{C_2}} + U_{\mathrm{CPD}}^{\mathrm{dark}}.$$

Here, $U_{\mathrm{CPD}}^{\mathrm{dark}}$ is defined as the CPD signal in the dark before starting the first illumination, A_1 and A_2 are the preexponential factors, B_1 and B_2 are the characteristic time constants, and C_1 and C_2 are the stretching exponents. In the following, we show and discuss mainly the time constants B_1 and B_2. The other fit parameters A_1 and A_2 (amplitudes of the two processes) as well as C_1 and C_2 (stretching exponents) have also been systematically determined and show a complicated dependence on illumination and intensity. The same fitting procedure was also applied to the conductivity data described below. The sum of A_1 and A_2 corresponds to the overall change of the CPD (and PC) and typical values for the stretching exponents are in range of 0.5 to 1, however, for some illumination conditions values larger than 1 have been observed. For quantitative fitting of the experimental data, different fitting functions were tried, however, a fit with stretched exponentials consistently gave the fits with the best quality both for the CPD and PC transients. So, we used this fitting procedure as a way to reveal differences between transients observed in the CPD and PC measurements, recorded when the light is switched on and off. Stretched exponential decays or Kohlrausch relaxations are frequently observed in many different processes in disordered systems and are caused by a continuous distribution of exponential relaxation processes [44,45]. In our case, the inherent disorder is expected to result for instance from a distribution of tunneling distances and/or potential fluctuations at the surface, which can be for example observed with Kelvin probe force microscopy (KPFM). As an example, we show in Fig. 2 the spatial variation of the CPD recorded under illumination over a scan size of 10 μm $\times$ 10 μm of the GaN surface. The microscopic variation of the surface potential according to Fig. 2 spans over 300 mV. As shall be shown in Fig. 3(a), the

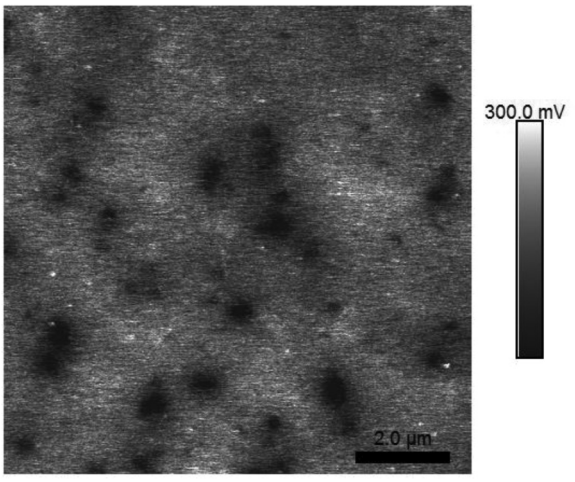

FIG. 2. Surface potential image (10 μm $\times$ 10 μm) obtained for the MOCVD grown GaN sample by KPFM under illumination with photons of 342 nm. The root mean square potential roughness of 50 mV is mainly caused by dislocations.

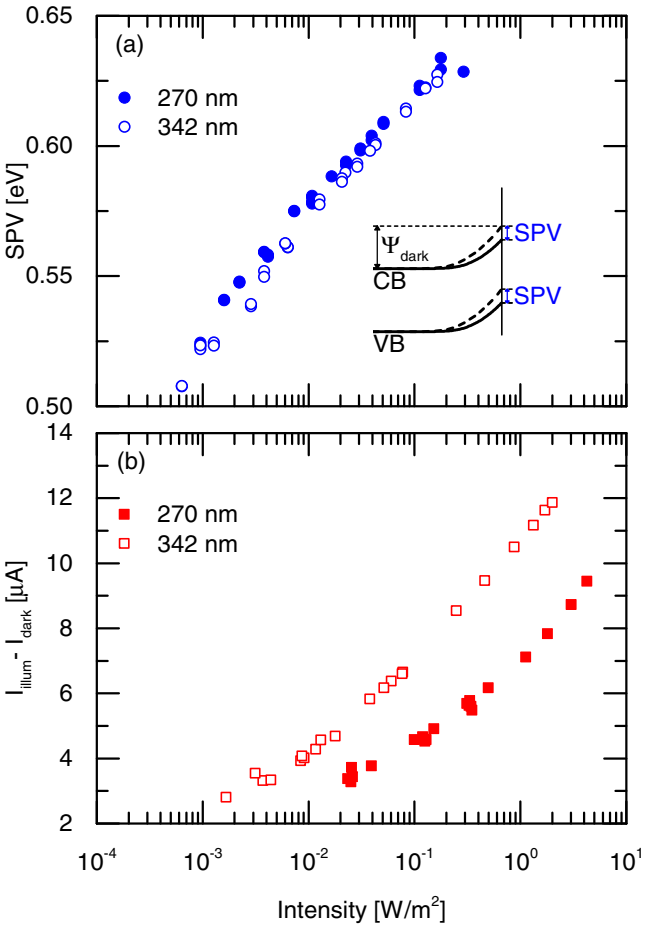

FIG. 3. (Color online) (a) Saturated SPV and (b) steady-state photocurrent as a function of the incident intensity for illumination with a wavelength of 270 nm (filled symbols) and with 342 nm (empty symbols). The SPV increases logarithmically with increasing intensity and no significant difference between the illumination with different wavelengths can be observed. The photocurrent also increases logarithmically with increasing intensity and, at a given intensity, is higher for illumination with the longer wavelength.

average SPV value observed for this sample in a macroscopic measurement is between 0.5 and 0.65 eV.

The results of the CPD measurements are shown in Fig. 3(a) for two illumination wavelengths as a function of the illumination intensity. The SPV increases logarithmically with increasing intensity as the band bending $\Psi = \Psi_{\mathrm{dark}} - \mathrm{SPV}$ becomes flatter. This is illustrated in the inset of Fig. 3(a), where the band bending in the dark Ψ_{dark} is represented by dashed lines and the band bending under illumination Ψ by solid lines. The SPV is indicated by a blue arrow in the inset of Fig. 3(a). No major difference is observed in the dependence of the SPV on light intensity for illumination with 270 and 342 nm photons. Foussekis *et al.* [19,21] also have observed an increase of the SPV with increasing light intensity and determined similar values for the SPV. In Fig. 4, the characteristic time constants (B_1 and B_2) for the decay of the CPD signal in the dark are shown as a function of the illumination intensity. Two different time constants, in the range of thousands of seconds and in the range of seconds, are

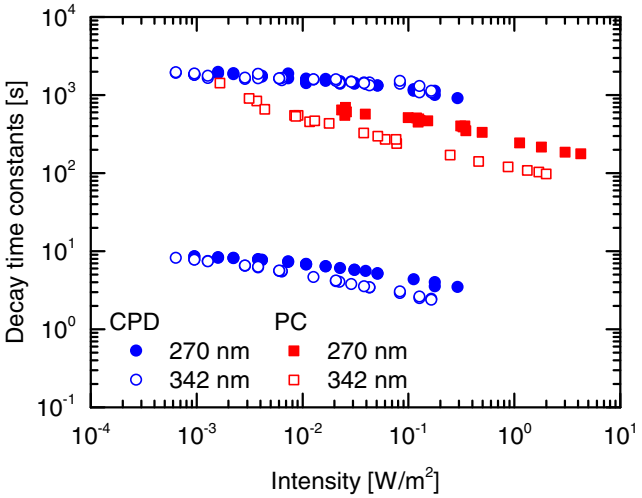

FIG. 4. (Color online) Decay time constants as a function of the incident light intensity for PC measurements (red squares) and for CPD measurements (blue circles) for illumination with light of 270 nm (filled symbols) and with light of 342 nm (empty symbols) wavelength. The decay for the photocurrent can be described by one time constant only, which decreases with increasing intensity. The decay of the CPD is described by two different time constants in the range of thousands of seconds and in the range of seconds. Both time constants show no clear dependence on the wavelength and decrease slightly with increasing intensity. The time constant for the decay of the PC decreases with increasing intensity from typically 1000 to 100 s and is smaller for the longer wavelength.

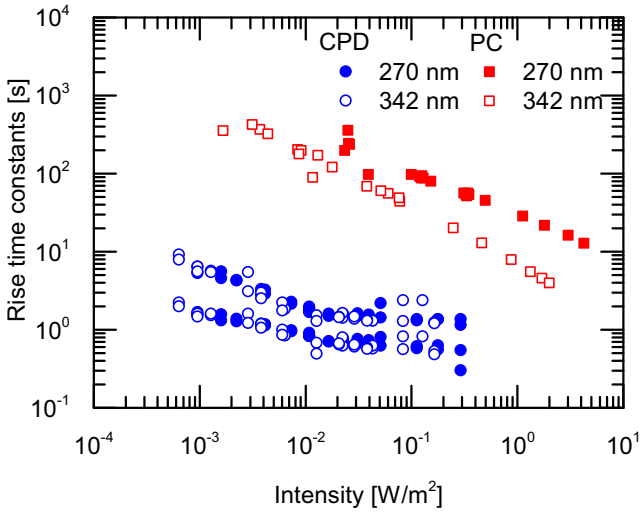

FIG. 5. (Color online) Rise time constants as a function of light intensity determined by PC measurements (red squares) and by CPD measurements (blue circles) for illumination with light of 270 nm (filled symbols) and with light of 342 nm (empty symbols) wavelength. With increasing intensity, the rise time of the photocurrent decreases, whereas the time constants for the CPD depend only weakly on the intensity and are in the range of seconds.

observed, which indicate that two processes are involved in the decay of the CPD signal after switching off the light. There is no major difference between the illumination with light of 270 and 342 nm wavelength. For both wavelengths, the two time constants decrease only weakly with increasing light intensity. The experimental data for the rise of the CPD signal under illumination could also be well described by two stretched exponential functions. From the fits, the characteristic time constants can be derived, which are shown as a function of light intensity in Fig. 5. The two time constants are very similar and have values in the range of seconds. Only a weak decrease of the time constants with increasing light intensity and no major difference between the two wavelengths is observed.

Previous studies of the CPD change with illumination carried out also in air but with freshly etched GaN surfaces reported a fast (few seconds time scale) rise of the CPD signal followed by a slow decrease [19,21]. We observe in our measurements a fast increase of the CPD signal immediately after the light is switched on, similar to the previous studies [19,21], but do not observe the reported slow decrease of CPD upon prolonged illumination of the sample. The same authors observed also that this CPD decrease is smaller if the samples were subjected to UV illumination in an oxygen environment prior to the experiments. The CPD decrease has been attributed to photoinduced adsorption of oxygen to the freshly etched GaN surface [19,21]. Electrons are transferred from the bulk to this surface oxygen, which results in a decrease of the CPD signal. In our case, the surface of GaN samples is already oxidized and, therefore, this effect is not observed. The surface oxide inhibits the interaction with oxygen molecules from air and, therefore, our data are instead similar to the data recorded in vacuum in the previous studies [19,21], where only the initial fast increase of CPD is observed. In those studies, also a slow decrease of the CPD after the illumination is switched off has been observed [19,21,22]. In some cases, this slow decrease seemed to display a logarithmic decay behavior, which agreed with a model for the time dependence of the CPD decay that considers thermionic emission of electrons from the bulk to surface states [20]. However, this model could not describe correctly the CPD decay in all cases [20,21]. In our data (Fig. 4), in addition to the slow decay reported previously [19–22], we also observe a fast decay component of the CPD, which has not been resolved in the previous studies using similar techniques. These observations will be discussed in more detail in the following.

For the PC measurements, a constant voltage of 0.1 V was applied to the Ohmic contacts (contact separation 4 mm) and the time-dependent current $I(t)$ was measured. In Fig. 1(b), data obtained from a typical PC measurement are shown. The current $I(t)$ is measured initially in the dark for 1 min. Then, the sample is illuminated until the current saturates and afterwards the decay of the current in the dark is measured for 30 min. For different illumination intensities, different illumination times were needed to reach a saturation of the photocurrent. The experimental data for the current rise under illumination and current decay after the illumination is switched off could be well described by one single stretched exponential function. The fits provide the saturation current under illumination I_{illum} and the saturation current in the dark I_{dark} as well as the characteristic time constants for the current rise under illumination and the current decay in the dark. The photocurrent is determined as $I_{\mathrm{illum}} - I_{\mathrm{dark}}$. This is shown as a function of the light intensity for illumination with

two different wavelengths in Fig. 3(b). The photocurrent also increases logarithmically with increasing intensity. At equal light intensity, the photocurrent is higher for the illumination with the longer wavelength. The light intensity dependence of the decay and rise times of the current are shown in Figs. 4 and 5, respectively, for illumination with light of different wavelengths. With increasing intensity, the decay and the rise times decrease from typically 1000 to 100 and 10 s, respectively. Our experimental data are in agreement with previous studies, which also described the decay of the photocurrent in the dark with one single stretched exponential function and determined similar values for the decay time in the range of hundreds to thousands of seconds [9,16,38,42]. However, these studies did not evaluate the behavior of the rise of the current under illumination and focused more on the dependence of the photocurrent on the photon energy of the illumination.

To help understanding our data and the processes taking place at the GaN surface, a schematic view of the electronic structure near the surface of GaN immediately after starting the illumination is shown in Fig. 6(a). The electronic structure is shown to scale and is based on the numerical simulation described in the following. In the dark, there is an upward surface band bending of approximately 1 eV due to electrons captured by surface states [23–26]. The numerical simulation of the band structure was performed in one dimension along the GaN growth direction with the help of the **nextnano**^{3} software package [46]. Here, the Schrödinger and Poisson equations are solved in a self-consistent way. The band bending induced by surface states is simulated by using an n-p-structure, where a thin (0.1 nm) p-type layer represents the effect of acceptor surface states. A surface charge density of 0.55×10^{12} cm^{-2} results in an upward band bending of approximately 1 eV and a SCR width of 100 nm. In addition to these surface states, we include a deep and a shallow defect band in our model. The deep defect band is centered approximately 2.2 eV below the CB and corresponds to the defects causing the YL, which is commonly observed in GaN [10,11]. This deep defect band is illustrated in yellow in Fig. 6. Moreover, numerous studies can also be found in the literature investigating shallow defects in GaN. With different techniques such as deep level transient spectroscopy (DLTS), thermally stimulated current (TSC), thermal and optical admittance spectroscopy (TAS and OAS), GaN layers grown by different methods such as molecular-beam epitaxy (MBE) [47–50], metal-organic and hybride phase epitaxy [51–56], and MOCVD [57,58] were investigated. Independent of the growth method or measurement technique, shallow defect states were found below the CB. Thus, a shallow defect band is also included in our scheme and illustrated in gray in Fig. 6(a). Localized states in this defect band are depicted by horizontal black lines. In the dark, the deep defect band is completely filled, whereas the surface states and the shallow defect band are filled up to the Fermi level E_F. As the deep defect band is well below the CB edge, we assume in the following discussion that mainly shallow defects are involved in the observed kinetics of the SPV and PC.

Under illumination, electrons can be excited from surface states to the CB (process A) or electron-hole pairs are generated. The electrons may recombine directly (process 1),

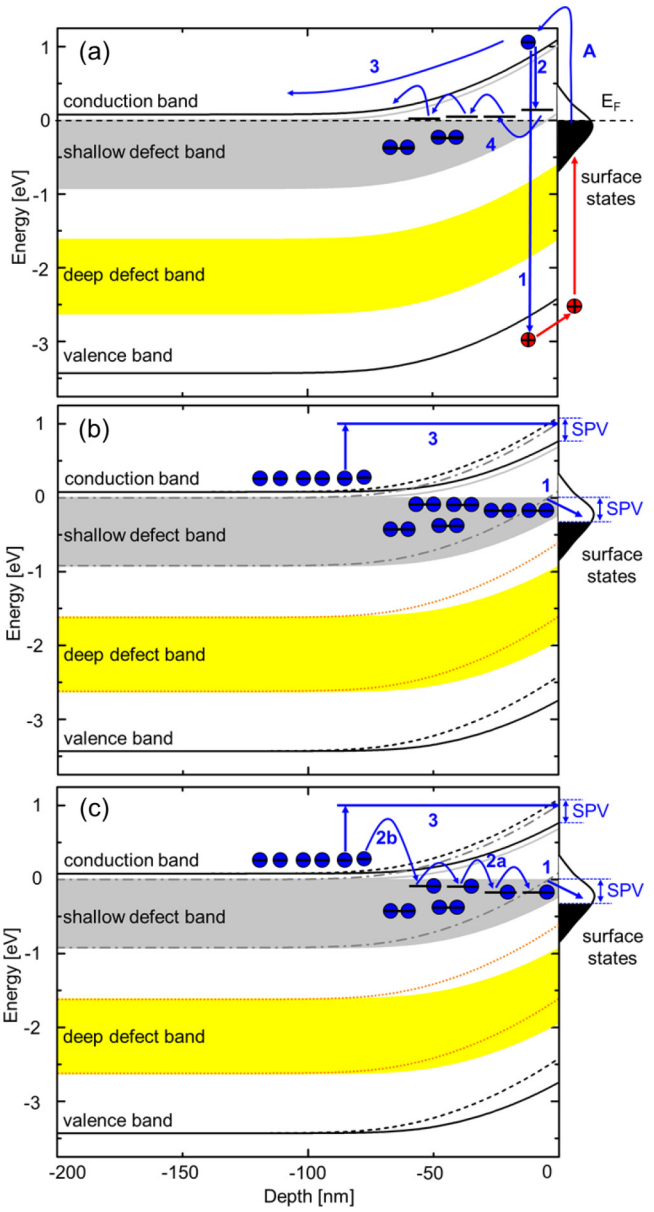

FIG. 6. (Color online) Schematic view of electronic structure near the surface of GaN immediately after starting the illumination (a) as well as immediately (b) resp. a few seconds (c) after stopping the illumination (band bending under illumination is represented by the solid line, whereas the band bending in the dark is represented by the dashed line). Furthermore, a shallow defect band located below the CB and a deep defect band centered around 2.2 eV below the CB are represented in gray and yellow, respectively. Electrons (holes) are shown in blue (red). The possible recombination processes are illustrated with blue arrows.

may be transferred back to the surface directly via thermionic emission or tunneling, may be trapped in empty localized states in the shallow defect band near the surface (process 2), or may drift or diffuse directly to the bulk via CB states (process 3).

Generated holes will drift to the surface and compensate electrons in surface states. The additional negative charge in the SCR and the more positive charge in the surface states causes the observed decrease of the surface band bending.

With CPD measurements, we monitor these changes in the charge density close to the surface. With PC measurements, we monitor the excitation of long-lived electrons to CB states outside the SCR. In Fig. 5, we have shown that the rise times of the CPD, which correspond to the removal of electrons from the surface, is in the range of seconds, whereas the time needed for the photocurrent to saturate under illumination, corresponding to the increase of the electron density in the CB, is in the range of hundreds of seconds (for low intensities). The change of the charge density at the surface results from the fast capture of holes by surface states, with the corresponding amount of electrons remaining inside the GaN. These electrons may be trapped in localized states in the shallow defect band near the surface (process 2) or drift and diffuse to the bulk (process 3). If process 3 would dominate, the rise time scales of the PC and CPD measurements should be similar as each time a hole is captured at the surface, an electron is simultaneously transferred into the CB outside the SCR. This does not correspond to our observations (see Fig. 5). Therefore, the dominant process is the fast trapping of electrons in localized states in the shallow defect band (process 2). The observed increase of the photocurrent on a much longer time scale, therefore, results from trapped electrons being transferred via localized states to the CB outside the SCR (process 4).

By fitting the data shown in Fig. 5, we observe that the rise time constant of the photocurrent decreases like the inverse square root of the light intensity for strongly absorbed light (270 nm). With increasing intensity, a larger number of electrons is excited into states which are located deeper in the material. These states are closer to the edge of the SCR and closer in energy to the CB. The probability for thermal excitation of these electrons from localized states to the CB outside the SCR and, thus, the probability for transfer into the bulk is larger. As a consequence, a shorter time is needed to reach the saturated photocurrent. We will show later that for sub-band-gap light (470 nm) the rise time constant is inversely proportional to the light intensity (see Fig. 10).

Next, the processes taking place immediately after switching off the light are discussed. Figures 6(b) and 6(c) illustrate the electronic structure near the surface in steady state under illumination and the processes that may take place, respectively, immediately and a few seconds after the illumination is switched off. To approach the dark state again, electrons captured in localized states in the shallow defect band are transferred to surface states, as these are energetically located at least partly below the shallow defect band. Electrons trapped in localized states near the surface may go directly to surface states (process 1), whereas electrons trapped in localized states deeper in the semiconductor have first to be transferred via hopping over localized states to the near surface states (process 2a). Electrons from the CB can either be trapped first at the edge of the SCR (process 2b) and then reach the surface also via process 2a or are directly transferred back to the surface via thermionic emission (process 3). In Fig. 4, we observe that the decay of the CPD signal is described by two different time constants, indicating a slow and a fast process, which do not depend significantly on light intensity. Immediately after switching off the illumination [see Fig. 6(b)], localized states in the shallow defect band are occupied up to the position of the Fermi level in the dark and, therefore, only processes 1 and 3 may take place as process 2 requires available empty states in the shallow defect band close in energy to the CB edge outside the SCR [see Fig. 6(c)]. Thus, we conclude that the fast process corresponds to electrons going from localized states directly to surface states (process 1), whereas the slow process includes the transfer of electrons trapped deeper in the semiconductor to the surface (process 2 or 3), which is, therefore, much slower than the direct process. In comparison, the decay of the photocurrent monitors the removal of electrons from the CB. Electrons from the CB can be removed by either hopping to the surface states across the entire SCR (process 2) or by thermionic emission (process 3). The decay time for the photocurrent decreases with increasing intensity (see Fig. 4). For increasing illumination intensity, the band bending becomes flatter, which corresponds to a lower and a thinner effective barrier for the hopping or thermionic emission of electrons. In the case of process 2, the transfer time most likely is limited by the last hopping process before process 1 takes place, which corresponds to the hopping process with the largest barrier. With increasing light intensity, the band bending and thus the barrier decreases, leading to a shorter time for the decay of the current in the dark.

In contrast, previous studies investigating the SPV or PPC only considered the process of thermionic emission and no transfer via hopping over localized states has been considered in the recovery of the surface band bending and of the photocurrent after switching off the illumination [12,13,19–22,36]. In order to further investigate the contributions of these two different processes, namely, thermionic emission and hopping via localized states, we further analyzed our data. Garrido *et al.* [12,13] have proposed a dynamic model for describing the decay of the photocurrent after switching off the illumination. This model takes into account two competing processes, the electron thermionic emission (I_{emiss}) from surface states and the thermionic capture (I_{cap}) over the barrier represented by the surface band bending from the bulk. This model neglects the effect of tunneling or hopping transport. In other words, this model only considers process 3, whereas process 2 is neglected. According to Garrido *et al.* [12], the dynamic equation of the accumulated surface charge $Q(t)$ can be expressed as

$$\frac{dQ(t)}{dt} = I_{\mathrm{cap}} - I_{\mathrm{emiss}} = AT^2 e^{-\Psi_{\mathrm{dark}}/V_T}\left[e^{\mathrm{SPV}(t)/V_T} - 1\right]$$

with

$$\mathrm{SPV}(t) = \Psi_{\mathrm{dark}} - \frac{Q(t)^2}{2e\epsilon_0\epsilon_r N_d}$$

and

$$Q(t=0) = \left[2e\epsilon_0\epsilon_r N_d\left(\Psi_{\mathrm{dark}} - \mathrm{SPV}\right)\right]^{\frac{1}{2}},$$

where A is the Richardson constant, e is the electron charge, $\epsilon_0\epsilon_r$ is the permittivity of the material, N_d the doping concentration, and V_T the thermal energy in eV.

With the help of this model it is possible to determine the surface photovoltage SPV by fitting the decrease of the current in the dark. Figure 7 shows the calculated photovoltage values as a function of the light intensity for both wavelengths, together with the SPV values measured by CPD. It can be seen that the calculated values are by a factor of 5 smaller than the experimentally determined values for the SPV but

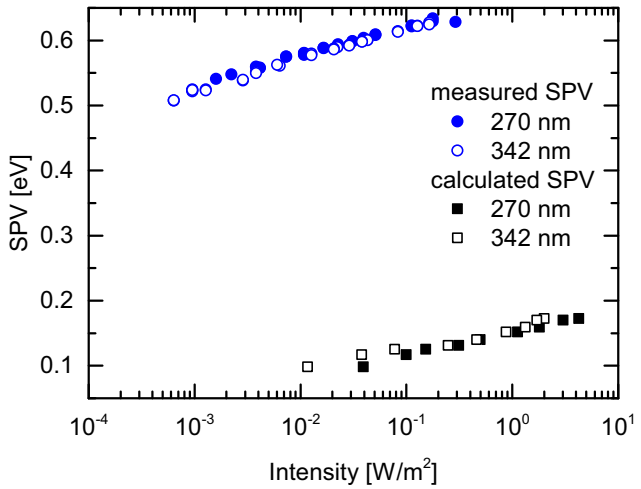

FIG. 7. (Color online) Calculated (black) and experimentally determined (blue) SPV as a function of the incident intensity for illumination with a wavelength of 270 nm (filled symbols) and with 342 nm (empty symbols).

show a similar intensity dependence. If thermionic emission (process 3) would be the dominant process for the recovery of the photocurrent in the dark, one would expect similar values for the calculated and experimentally measured values of the SPV. As the experimentally measured SPV values are higher, thermionic emission alone cannot explain our experimental observations.

This is also supported by PC decay measurements carried out at different temperatures. In Fig. 8, the decay time constants are shown as a function of the light intensity at 342 nm for PC measurements performed at room temperature and at three elevated temperatures. The observed decrease of the decay time constants is only a factor of 2 to 4 when the temperature is increased by about 50 °C. Assuming that the temperature dependence of the decay time constant follows an exponential dependence

$$\tau_i = \tau_0 e^{-\frac{E_A}{kT_i}},$$

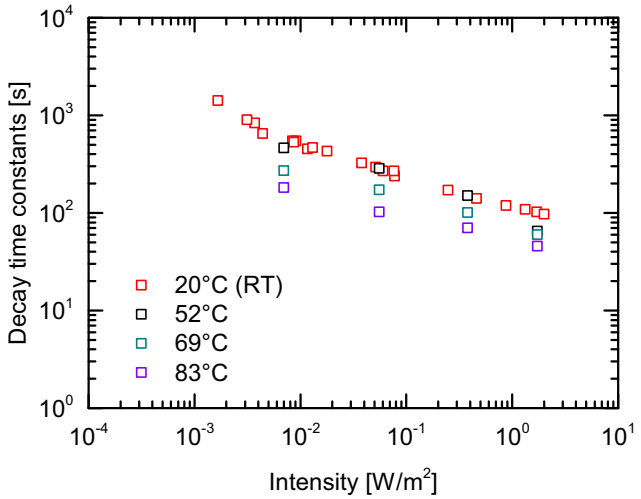

FIG. 8. (Color online) Decay time constants as a function of the incident light intensity obtained from PC measurements performed at different temperatures. The photon wavelength has been 342 nm.

where k is the Boltzmann constant and τ_0 and τ_i are the decay time constants at 0 K and at temperature T_i, respectively, the corresponding activation energy E_A can be calculated according to

$$E_A = -k\frac{T_1 T_2}{T_1 - T_2}\ln(\tau_1/\tau_2).$$

This activation energy corresponds to the effective barrier of charge removal from conduction band states. The experimentally determined barrier height is in the range of 100–200 meV for the whole range of illumination intensities. This leads to the conclusion that the effective barrier of charge removal from conduction band states does not correspond to the surface band bending height but rather to another (much smaller) barrier, which in Fig. 6(c) governs the time scale of process 2b.

We have demonstrated that electrons from conduction band states are first captured in localized states in the shallow defect band [process 2b in Fig. 6(c)]. After this, they move via localized states to surface states [process 2a in Fig. 6(c)]. The time of the recapture of electrons in surface states [governed by process 2a in Fig. 6(c)] is determined by the hopping between localized states in the shallow defect band, which depends on the density of these defects. The density of these states required to have the observed charge transfer time scales of about 1000 s, obtained from the decay of the CPD transients after the light is switched off, may be estimated. For this estimation, we assume that hopping corresponds to a sequence of tunneling processes, where the electrons move from one defect state to another by tunneling through a rectangular barrier, whose width corresponds to the spatial distance between the defect states. The inverse decay time follows:

$$\frac{1}{t_{\text{decay}}} = f_{\text{phonon}} P$$

with

$$P \simeq \frac{16E(U-E)}{U^2}\exp\left(-2\sqrt{\frac{2m^*(U-E)}{\hbar^2}}W\right),$$

where f_{phonon} is a typical phonon frequency of 750 cm^{-1} as the attempt to tunnel frequency in thermally activated processes. P is the tunneling probability [59] for electrons with an energy at room temperature of $E = 0.025$ eV. The constant $\hbar$ is the reduced Planck constant. The height of the tunneling barrier is $U = 0.2$ eV and its width is W. Assuming that each defect is at the center of a sphere with radius $W/2$, the defect density can be estimated as $[\frac{4}{3}\pi(\frac{W}{2})^3]^{-1}$. Taking the effective mass of electrons in wurtzite GaN of $m^* = 0.2\,m_0$ (m_0 is the free-electron mass), we estimate from this calculation a density of defect states of the order of 10^{17} cm^{-3}, which is in the range of defect densities typically present in GaN films.

Furthermore, CPD and PC measurements were performed on the same sample using below band-gap (visible) light. Under illumination with visible light, in our case with a wavelength of 470 nm, electrons can either be directly excited from surface states to the CB or electron and hole excitation in the bulk can take place. Illuminating the sample with visible light (470 nm) also leads to a measurable change of the CPD and the PC. Figures 9(a) and 9(b) show the measured CPD and PC as a function of time for illumination with light of 270 nm

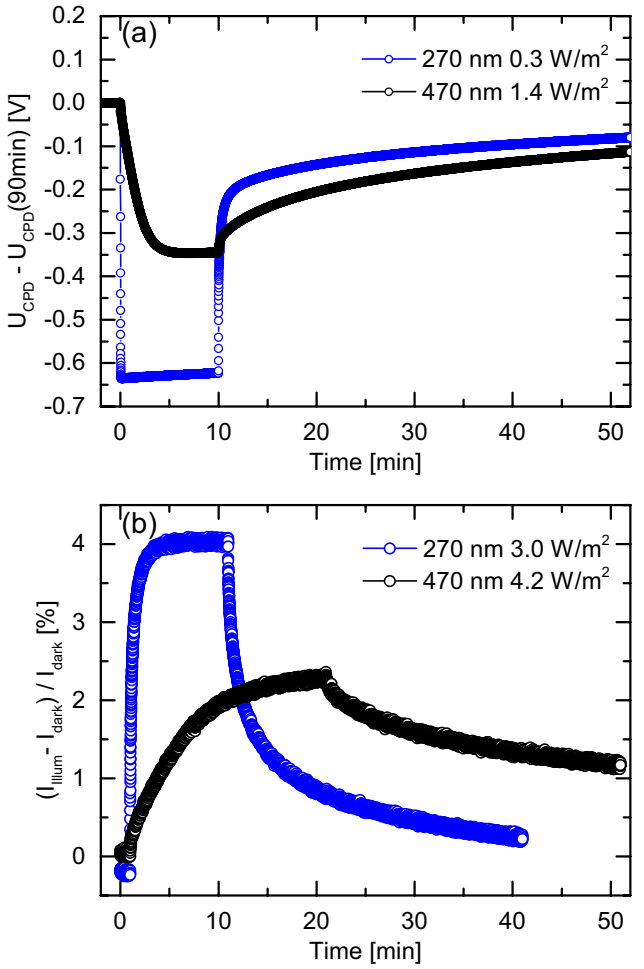

FIG. 9. (Color online) (a) CPD and (b) PC recorded as a function of time for illumination with light of 270 nm (blue symbols) and with light of 470 nm (black symbols) for comparable illumination intensities (indicated).

(blue symbols) and with light of 470 nm (black symbols) for similar illumination intensities. The observed changes under illumination with visible light are at a similar intensity by a factor of 2 smaller compared to the UV illumination.

Comparing the rise times for illumination with above and below band-gap light (see Fig. 10), one obtains similar values for the rise time of the photocurrent (in the range of hundreds of seconds), whereas there is a significant difference for the rise times of the CPD. Under UV illumination, the two rise times of the CPD are similar and lie in the range of seconds. For illumination with visible light, two different time scales are obtained, one in the range of seconds, similar to case of UV illumination, and a much larger second time scale in the range of hundreds of seconds. We conclude that for illumination with visible light, the excited electrons are also trapped in localized states, as the rise time of the photocurrent is similar for both illuminations. The change of the CPD under illumination was attributed to the drift of generated holes to the surface and the trapping of electrons in localized shallow states close to the surface. Both processes are fast and exhibit time scales in the range of seconds. The differences in the CPD measurements for visible light can be explained by the

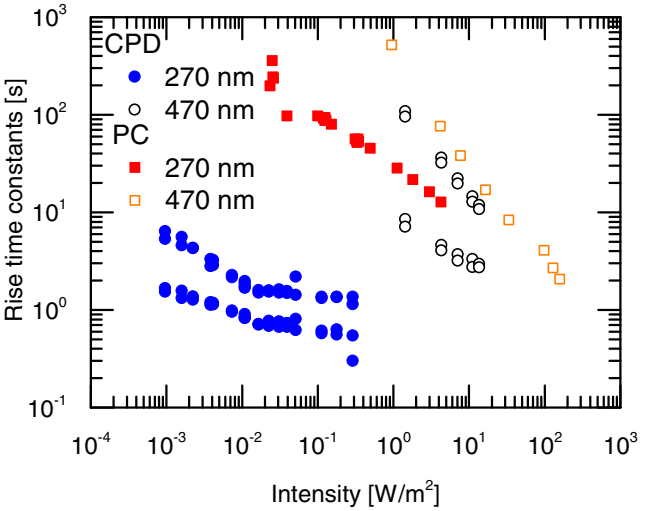

FIG. 10. (Color online) Rise time constants as a function of the incident light intensity determined in PC measurements (squares) and in CPD measurements (circles) for illumination with light of 270 nm (filled symbols) and with light of 470 nm (empty symbols) wavelength.

excitation of holes far away from surface states. In the case of visible light, holes are mostly excited in the bulk and, therefore, the capture of photoholes at the surface is less efficient than in the case of holes generated with UV illumination (close to the surface), where electron-hole separation can take place more efficiently due to the surface band bending. The less efficient capture of holes explains the smaller observed SPV values and the longer time scale of the rise of the CPD.

A comparison of the decay times (see Fig. 11) shows that similar values between 270 and 470 nm illumination are obtained for the PC and CPD measurements. The decay of the PC was attributed to hopping of CB electrons to the surface

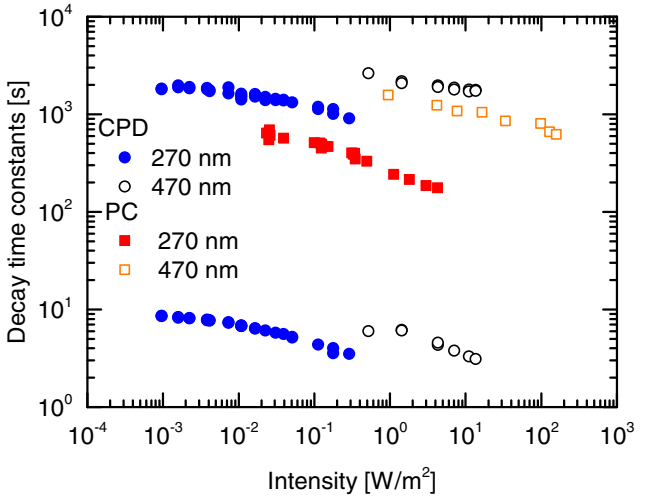

FIG. 11. (Color online) Decay time constants as a function of the incident intensity determined in PC measurements (squares) and in CPD measurements (circles) for illumination with light of 270 nm (filled symbols) and with light of 470 nm (empty symbols) wavelength.

TABLE I. Comparison of unintentionally MOCVD and Si-doped MBE grown samples. CPD and PC measurements were performed with light of 342 nm wavelength and an illumination intensity of 4–5 mW/m^2.

Sample growth technique	Carrier concentration (cm^{-3})	Charge mobility (cm^2/Vs)	$\frac{I_{illum} - I_{dark}}{I_{dark}}$	PC rise time (s)	PC decay time (s)	SPV (eV)	CPD rise time (s)	CPD decay time (s)
MOCVD	1.4×10^{17}	170	0.0134	370	830	0.55	2.8 1.1	1750 6
MBE	1.6×10^{19}	35	0.0053	53 6.5	130	0.25	135 5	1350 7

states across the entire SCR. The observation of two different time scales of the CPD, one in the range of seconds and the other one in the range of thousands of seconds, was explained by the fast process of trapped electrons going directly to surface states and the slow process of electrons trapped in localized states deeper in the semiconductor being transferred via hopping to the surface states. As similar time constants are observed for the illumination with visible light, it can be concluded that the same processes take place. However, the relative contribution of the two processes is different for the illumination with above and below band-gap light. After switching off the UV light, the slow and the fast processes exhibit similar contributions, whereas after switching off the visible light, the contribution of the fast process is a factor of 10 smaller than the contribution of the slow process. Thus, less electrons are trapped in the shallow localized states in the SCR and more electrons are excited in the bulk compared to the direct excitation of electrons from surface states.

Furthermore, to show the general relevance of our model, an intentionally Si-doped (0001) GaN layer grown by plasma-assisted MBE was investigated. This MBE sample exhibits a carrier concentration of 1.6×10^{19} cm^{-3} and an electron mobility of 35 cm^2/Vs measured by Hall effect. PC and CPD measurements for illumination with a wavelength of 342 nm were performed on this sample. Table I shows a comparison between data obtained for the MOCVD and Si-doped MBE grown samples from measurements carried out with light of 342 nm wavelength and an illumination intensity of 4–5 mW/m^2.

Comparing the short time scale of the decay of the CPD signal (6 s for the MOCVD sample and 7 s for the MBE sample), we can see that for both samples this fast process takes place on a similar time scale. Thus, for both samples, electrons move directly from localized states of the shallow defect band to surface states [process 1 in Figs. 6(b) and 6(c)]. From the decay time scales of the PC and CPD measurements obtained for the MBE sample, one can see that the decay time constant of the CPD is much larger (1350 s) than the decay time constant of the PC (130 s). Therefore, we conclude that also for the MBE sample no direct transfer of conduction band electrons to surface states takes place as in the case of the MOCVD sample.

For the MBE sample, one time scale of the rise of the PC under illumination (6.5 s) is similar to one time scale of the rise of the CPD (5 s). Thus, we conclude that the direct transfer of electrons to conduction band states [process 3 in Fig. 6(a)] occurs in the case of the MBE sample. However, a second longer time scale is observed for the PC and the CPD rise under illumination (53 and 135 s, respectively). Although we cannot be sure at this point and more studies have to be performed, we believe that these long time scales are due to an inefficient separation of photogenerated electrons and holes in the MBE sample. These long rise time scales of the PC and the CPD obtained for the MBE sample are in the same range as the values obtained for the MOCVD sample for illumination with below band-gap light of similar illumination intensity. In the case of the MBE sample, the width of the SCR is smaller due to the higher doping concentration and, therefore, electron-hole pairs are mostly excited outside the SCR. Thus, in both cases electrons and holes are mostly excited outside the SCR, where there is no band bending and electron-hole separation is inefficient, resulting in the observed long time scales. The influence of doping on the kinetics of photogenerated charges will be studied in detail in a following work.

In summary, qualitatively similar behavior is observed for samples grown by different techniques and with different doping levels. However, the corresponding time constants are expected to depend on doping level and defect density.

IV. CONCLUSIONS AND OUTLOOK

By combining PC and CPD measurements under identical conditions for the same sample, valuable information can be obtained about the kinetics of charges photogenerated at the GaN surface. We have compared the processes involved in the excitation and decay of charge carriers generated by above (UV) and below (visible) band-gap light with varying light intensity, where electrons and holes are generated close to and far away from the surface. In particular, we have probed the role played by localized shallow defect states in the kinetics of photogenerated charges. These states are responsible for the trapping of photogenerated electrons in the SCR close to the surface, which explains the slow response of the photocurrent. These states are also involved in the transfer of electrons back to the surface after illumination, which results in the slow recovery of the CPD response after illumination. Moreover, due to the presence of these defect levels, both electrons and holes can be generated (far from the surface) with below band-gap light. However, capture of photoholes at the surface is in this case less efficient than in the case of holes generated with UV illumination (close to the surface), where electron-hole separation can take place more efficiently due to surface band bending. In contrast, thermionic emission so far discussed in the literature only plays a minor

role. This is also demonstrated by the temperature dependence of the decay time constants. According to our measurements, the barrier height that electrons have to overcome to be removed from CB states is approximately 100–200 meV, which is much smaller than the band bending height under illumination. For Si-doped GaN samples grown by MBE we observe qualitatively similar behavior. However, the corresponding time constants are expected to depend on doping level and defect density. A detailed comparison between the MOCVD and MBE grown samples and the influence of doping is beyond the scope of this study and will be reported elsewhere.

ACKNOWLEDGMENTS

Financial support from TUM.solar in the frame of the Bavarian Collaborative Research Project "Solar technologies go Hybrid" (SolTec) and the Excellence Cluster Nanosystems Initiative Munich is gratefully acknowledged. The authors acknowledge Stefan Birner for **nextnano**^{3} support.

[1] H. Morkoç and S. N. Mohammad, Science **267**, 51 (1995).
[2] M. S. Shur, Solid State Electron. **42**, 2131 (1998).
[3] G. Y. Xu, A. Salvador, W. Kim, Z. Fan, C. Lu, H. Tang, H. Morkoç, G. Smith, M. Estes, B. Goldenberg, W. Yang, and S. Krishnankutty, Appl. Phys. Lett. **71**, 2154 (1997).
[4] J. Howgate, S. J. Schoell, M. Hoeb, W. Steins, B. Baur, S. Hertrich, B. Nickel, I. D. Sharp, M. Stutzmann, and M. Eickhoff, Adv. Mater. **22**, 2632 (2010).
[5] S. Schäfer, S. A. Wyrzgol, R. Caterino, A. Jentys, S. J. Schoell, M. Hävecker, A. Knop-Gericke, J. A. Lercher, I. D. Sharp, and M. Stutzmann, J. Am. Chem. Soc. **134**, 12528 (2012).
[6] H. S. Jung, Y. J. Hong, Y. Li, J. Cho, Y.-J. Kim, and G.-C. Yi, ACS Nano **2**, 637 (2008).
[7] M. G. Kibria, H. P. T. Nguyen, K. Cui, S. Zhao, D. Liu, H. Guo, M. L. Trudeau, S. Paradis, A.-R. Hakima, and Z. Mi, ACS Nano **7**, 7886 (2013).
[8] J. W. Ager, L. A. Reichertz, Y. Cui, Y. E. Romanyuk, D. Kreier, S. R. Leone, K. M. Yu, W. J. Schaff, and W. Walukiewicz, Phys. Status Solidi C **6**, S413 (2009).
[9] H. M. Chen, Y. F. Chen, M. C. Lee, and M. S. Feng, J. Appl. Phys. **82**, 899 (1997).
[10] H. M. Chen, Y. F. Chen, M. C. Lee, and M. S. Feng, Phys. Rev. B **56**, 6942 (1997).
[11] I. Shalish, L. Kronik, G. Segal, Y. Rosenwaks, Y. Shapira, U. Tisch, and J. Salzman, Phys. Rev. B **59**, 9748 (1999).
[12] J. A. Garrido, E. Monroy, I. Izpura, and E. Muñoz, Semicond. Sci. Technol. **13**, 563 (1998).
[13] E. Muñoz, E. Monroy, J. A. Garrido, I. Izpura, F. J. Sanchez, M. A. Sanchez-Garcia, E. Calleja, B. Beaumont, and P. Gibart, Appl. Phys. Lett. **71**, 870 (1997).
[14] C. Johnson, J. Y. Lin, H. X. Jiang, M. A. Khan, and C. J. Sun, Appl. Phys. Lett. **68**, 1808 (1996).
[15] M. T. Hirsch, J. A. Wolk, W. Walukiewicz, and E. E. Haller, Appl. Phys. Lett. **71**, 1098 (1997).
[16] C. H. Qiu and J. I. Pankove, Appl. Phys. Lett. **70**, 1983 (1997).
[17] C. V. Reddy, K. Balakrishnan, H. Okumura, and S. Yoshida, Appl. Phys. Lett. **73**, 244 (1998).
[18] M. Foussekis, A. A. Baski, and M. A. Reshchikov, Appl. Phys. Lett. **94**, 162116 (2009).
[19] M. Foussekis, J. D. Ferguson, A. A. Baski, H. Morkoç, and M. A. Reshchikov, Physica B (Amsterdam) **404**, 4892 (2009).
[20] M. A. Reshchikov, M. Foussekis, and A. A. Baski, J. Appl. Phys. **107**, 113535 (2010).
[21] M. Foussekis, A. A. Baski, and M. A. Reshchikov, J. Vac. Sci. Technol. B **29**, 041205 (2011).
[22] J. D. Wei, S. F. Li, A. Atamuratov, H.-H. Wehmann, and A. Waag, Appl. Phys. Lett. **97**, 172111 (2010).
[23] V. M. Bermudez, J. Appl. Phys. **80**, 1190 (1996).
[24] G. Koley and M. G. Spencer, J. Appl. Phys. **90**, 337 (2001).
[25] C. I. Wu, A. Kahn, N. Taskar, D. Dorman, and D. Gallagher, J. Appl. Phys. **83**, 4249 (1998).
[26] S. Sabuktagin, M. A. Reshchikov, D. K. Johnstone, and H. Morkoç, Mat. Res. Soc. Symp. Proc. **798**, Y5.39 (2004).
[27] D. Goguenheim and M. Lannoo, Phys. Rev. B **44**, 1724 (1991).
[28] K. A. Bulashevich and S. Y. Karpov, Phys. Status Solidi C **3**, 2356 (2006).
[29] W. E. Spicer, P. W. Chye, P. R. Skeath, C. Y. Su, and I. Lindau, J. Vac. Sci. Technol. **16**, 1422 (1979).
[30] H. Hasegawa, L. He, H. Ohno, T. Sawada, T. Haga, Y. Abe, and H. Takahashi, J. Vac. Sci. Technol. B **5**, 1097 (1987).
[31] K. Prabhakaran, T. G. Andersson, and K. Nozawa, Appl. Phys. Lett. **69**, 3212 (1996).
[32] I. Shalish, Y. Shapira, L. Burstein, and J. Salzman, J. Appl. Phys. **89**, 390 (2001).
[33] J. P. Long and V. M. Bermudez, Phys. Rev. B **66**, 121308 (2002).
[34] M. A. Reshchikov, S. Sabuktagin, D. K. Johnstone, and H. Morkoç, J. Appl. Phys. **96**, 2556 (2004).
[35] H. Sezen, E. Ozbay, O. Aktas, and S. Suzer, Appl. Phys. Lett. **98**, 111901 (2011).
[36] I. Shalish, L. Kronik, G. Segal, Y. Shapira, S. Zamir, B. Meyler, and J. Salzman, Phys. Rev. B **61**, 15573 (2000).
[37] J. Z. Li, J. Y. Lin, H. X. Jiang, A. Salvador, A. Botchkarev, and H. Morkoç, Appl. Phys. Lett. **69**, 1474 (1996).
[38] J. Z. Li, J. Y. Lin, H. X. Jiang, M. A. Khan, and Q. Chen, J. Appl. Phys. **82**, 1227 (1997).
[39] J. Z. Li, J. Y. Lin, H. X. Jiang, M. A. Khan, and Q. Chen, J. Vac. Sci. Technol. B **15**, 1117 (1997).
[40] G. Beadie, W. S. Rabinovich, A. E. Wickenden, D. D. Koleske, S. C. Binari, and J. A. Freitas, Appl. Phys. Lett. **71**, 1092 (1997).
[41] W. Rieger, R. Dimitrov, D. Brunner, E. Rohrer, O. Ambacher, and M. Stutzmann, Phys. Rev. B **54**, 17596 (1996).
[42] V. V. Ursaki, I. M. Tiginyanu, P. C. Ricci, A. Anedda, S. Hubbard, and D. Pavlidis, J. Appl. Phys. **94**, 3875 (2003).
[43] L. Kronik and Y. Shapira, Surf. Sci. Rep. **37**, 1 (1999).
[44] F. R. Libsch and J. Kanicki, Appl. Phys. Lett. **62**, 1286 (1993).
[45] D. C. Johnston, Phys. Rev. B **74**, 184430 (2006).
[46] S. Birner, T. Zibold, T. Andlauer, T. Kubis, M. Sabathil, A. Trellakis, and P. Vogl, IEEE Trans. Electron Devices **54**, 2137 (2007).
[47] D. C. Look, Z. Q. Fang, W. Kim, O. Aktas, A. Botchkarev, A. Salvador, and H. Morkoç, Appl. Phys. Lett. **68**, 3775 (1996).

[48] A. Krtschil, H. Witte, M. Lisker, J. Christen, U. Birkle, S. Einfeldt, and D. Hommel, J. Appl. Phys. **84**, 2040 (1998).
[49] A. Krtschil, M. Lisker, H. Witte, J. Christen, U. Birkle, S. Einfeldt, and D. Hommel, Mater. Sci. Eng. B **59**, 226 (1999).
[50] A. Krtschil, H. Witte, M. Lisker, J. Christen, A. Krost, U. Birkle, S. Einfeldt, D. Hommel, F. Scholz, J. Off, and M. Stutzmann, Appl. Phys. Lett. **77**, 546 (2000).
[51] P. Hacke, T. Detchprohm, K. Hiramatsu, N. Sawaki, K. Tadatomo, and K. Miyake, J. Appl. Phys. **76**, 304 (1994).
[52] P. Hacke, A. Maekawa, N. Koide, K. Hiramatsu, and N. Sawaki, Jpn. J. Appl. Phys. **33**, 6443 (1994).
[53] W. I. Lee, T. C. Huang, J. D. Guo, and M. S. Feng, Appl. Phys. Lett. **67**, 1721 (1995).
[54] D. Haase, M. Schmid, W. Kurner, A. Dornen, V. Harle, F. Scholz, M. Burkard, and H. Schweizer, Appl. Phys. Lett. **69**, 2525 (1996).
[55] H. Witte, K. Fluegge, A. Dadgar, A. Krtschil, A. Krost, and J. Christen, Mat. Res. Soc. Symp. Proc. **798**, Y5.37 (2004).
[56] H. Witte, E. Schrenk, K. Flügge, A. Krost, J. Christen, B. Kuhn, and F. Scholz, Phys. Rev. B **71**, 125213 (2005).
[57] W. Götz, N. M. Johnson, H. Amano, and I. Akasaki, Appl. Phys. Lett. **65**, 463 (1994).
[58] W. Götz, N. M. Johnson, R. A. Street, H. Amano, and I. Akasaki, Appl. Phys. Lett. **66**, 1340 (1995).
[59] S. M. Sze and K. K. Ng, *Physics of Semiconductor Devices* (John Wiley & Sons, Inc., New Jersey, 2006).